Electro-optic Behavior of Liquid-Crystal-Filled Silica Opal Photonic Crystals: Effect of Liquid-Crystal Alignment

Daeseung Kang,[1,*] Joseph E. Maclennan,[1] Noel A. Clark,[1] Anvar A. Zakhidov,[2] and Ray H. Baughman[2]
[1]*Department of Physics, Ferroelectric Liquid Crystal Materials Research Center, University of Colorado, Boulder, Colorado 80309*
[2]*Materials Laboratory, Honeywell International Corporation, Morristown, New Jersey 07962-1021*
(Received 19 October 2000)

Photonic crystals made of nematic liquid crystal intercalated into the void space of close-packed silica spheres (synthetic porous opal) exhibit significant electric-field-induced shift of the optical Bragg reflection peak when the liquid crystal has the long molecular axis oriented parallel to the sphere surfaces. No such effect is observed for comparable fields when the long-axis orientation is normal to the sphere surfaces.

DOI: 10.1103/PhysRevLett.86.4052 PACS numbers: 61.30.Gd, 42.70.Df, 42.70.Qs

The search for and interest in structures exhibiting frequency gaps for the propagation of electromagnetic radiation has produced a rich variety of new optical and materials physics [1–4]. Many potential photonic crystal applications require electro-optic response, wherein, for example, applied electric field controls the Bragg reflectivity [5–7] of a photonic crystal. In this connection liquid crystals (LCs), which by themselves are among the most useful electro-optic materials [8], are of particular interest, and, indeed, the incorporation of LCs into two and three dimensional photonic band gap composite structures has begun to be explored [9–13].

Here we present a study of the structure and electro-optic behavior of hybrid LC-silica sphere photonic crystals, formed by filling the (26% by volume) void space of face centered cubic (fcc) crystals of silica spheres (synthetic porous opals) with nematic LC. We focus on surface interactions and their role in a nematic confined in a periodic, multiply connected, contiguous void space. The observation of a significant dependence of electro-optic response on surface alignment, along with strong hysteresis in the parallel alignment case, points to the role of topological defects in the LC orientation field.

The fcc opal crystals were made from silica spheres, of nominal diameter $D \approx 200$ nm [14], rendered nearly monodisperse in a fractionation process involving repeated centrifugation and dilution [15]. Crystal growth was carried out by slow sedimentation in water in a 10 μm thick gap between vertical indium-tin oxide (ITO) coated glass plates. The crystals grow with the [111] direction normal to the plates at a rate of $\sim$1 mm/day. Crystal rigidity was enhanced by thermal annealing for 12 h at 250 °C, after slow evaporation of the water at lower temperature. The expected fcc structure was confirmed by scanning electron microscopy of the dehydrated crystal with the glass removed. The uniaxially birefringent nematic LC Merck-PCH5 (isotropic $\leftarrow$ 54 °C $\rightarrow$ nematic) [16] was filled in the isotropic phase into the void space of the opal via capillarity in vacuum. Two LC alignment conditions were employed: *parallel*—the dehydration procedure just outlined gives "random planar" alignment on an amorphous silica surface, with $\mathbf{n}(\mathbf{r})$ parallel to the surface but of unspecified orientation in the surface plane; *normal*—prior to filling the fcc opal is soaked in 1% hexadecyltrimethylammonium-bromide in chloroform and then dried. The adsorption of this surfactant onto the silica produces "homeotropic" alignment, with $\mathbf{n}(\mathbf{r})$ locally normal to the surface [17].

Optical characteristics of the opals and of the opal/LC composites were studied using Bragg reflection microscopy [18] for incident white light, with a NA = 0.4 objective on a microscope equipped with an Ocean Optics S2000 spectrometer. The fcc crystal domain dimension was 50–100 μm in the plane of the plates. The fcc crystals were viewed at normal incidence to the plates in the [111] Bragg back-reflection geometry, so diffraction occurs at a wavelength $\lambda_B = D(2\sqrt{2/3})n$, where n is the mean refractive index of the medium.

Figure 1 shows the thermal and field-induced behavior of the [111] Bragg wavelength λ_B and the corresponding effective LC index n_{LCeff}. The [111] Bragg peak, shown in Fig. 1A, at $T = 45$ °C has HWHH $\sim$7.5 nm and maintains its basic shape upon both electric field application and temperature change. Assuming that the Bragg peak wavelength shift is caused by variation of the mean refractive index of the medium, determined from the volume average of the dielectric constants of the silica and LC, one obtains $\lambda_B = D(2\sqrt{2/3})\sqrt{0.74n_s^2 + 0.26n_{\mathrm{LCeff}}^2}$, where n_s is the silica refractive index, fixed at its typical bulk value $n_s = 1.45$. In order for n_{LCeff} to match the bulk LC value $n_{\mathrm{LC}} = 1.52$ in the isotropic phase at $T = 55$ °C, D is fixed at $D = 207$ nm, which is consistent with scanning electron microscopy measurement. With these values n_{LCeff} calculated from λ_B matches the bulk LC index in the isotropic T range and follows the isotropic average of the bulk nematic extraordinary and ordinary refractive indices, i.e., $n_{\mathrm{ave}} = \sqrt{(n_e^2 + 2n_o^2)/3}$ in the temperature range of nematic phase, for both parallel and normal alignment on the spheres. This is expected for an isotropic $\mathbf{n}(\mathbf{r})$ distribution in the limit where the silica-LC index difference is sufficiently small that there is only weak spatial

 0031-9007/01/86(18)/4052(4)$15.00

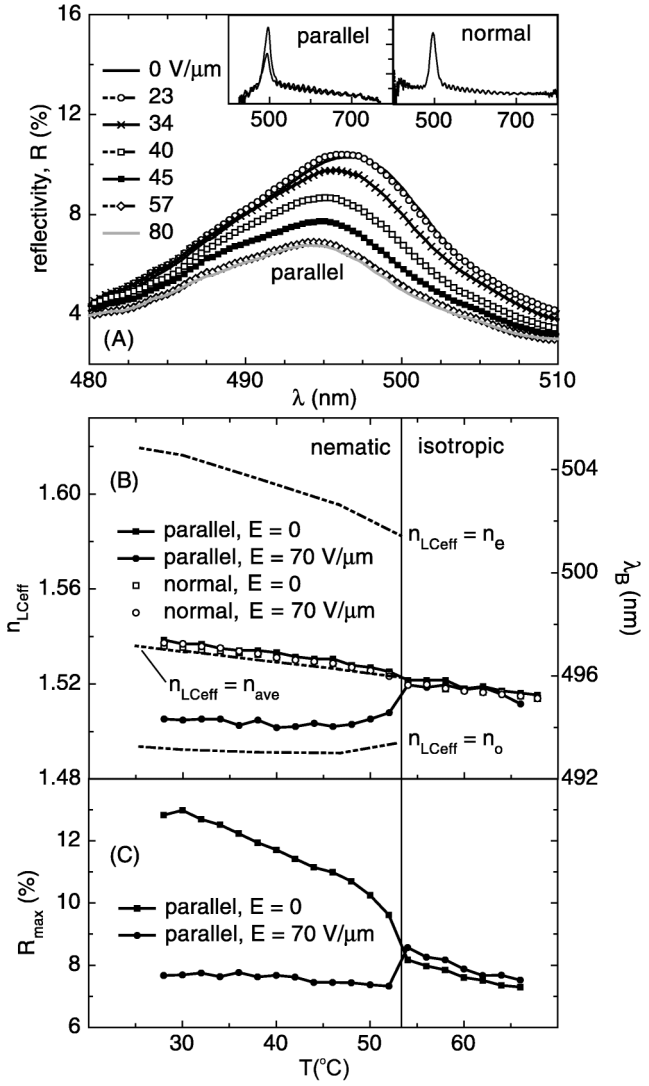

FIG. 1. (A) Reflection spectra of an opal crystal infiltrated with PCH5 for light incident parallel to a [111] direction, showing the [111] Bragg reflection peaks. For *parallel* alignment of LC on the spheres there is a field-induced shift of the Bragg reflection peak wavelength, whereas for *normal* alignment there is no shift for comparable fields. (B) Bragg peak wavelength λ_B and the corresponding effective LC refractive index n_{LCeff} vs temperature. The dotted curves show the maximum possible range of λ_B and n_{LCeff}, as the LC index varies from its minimum value n_o to its maximum value n_e, as well as n_{ave}, the mean bulk LC refractive index. (C) Peak Bragg reflectivity R_{max} vs T for the *parallel* case for $E = 0$ and $E = 70$ V/μm.

inhomogeneity of the optical electric field in the opal/LC lattice. Figure 1B also shows the Bragg wavelengths in the extreme cases where n_{LCeff} has its maximum value (n_e) and minimum (n_o) values. These limits represent the maximum possible field-induced excursion of λ_B in this composite system. Figure 1B also shows the temperature dependence of λ_B in both the parallel and normal cases with an applied field $E = 70$ V/μm, 60 Hz ac. As can be seen, this field produces little change in λ_B for the normal case, the normal $E = 70$ V/μm curve tracking exactly the normal and parallel $E = 0$ data in the nematic phase. In the parallel case, however, the applied field generates a distinct change in λ_B, producing ~60% of the maximum possible shift of n_{LCeff} toward n_o. This indicates that $\mathbf{n}(\mathbf{r})$ is reoriented parallel to E and normal to the ITO coated plates, as expected for the positive dielectric anisotropy of PCH5 ($\Delta\varepsilon = 12.7$) [16]. The optical electric field then is mostly normal to $\mathbf{n}(\mathbf{r})$ so n_{LCeff} approaches n_o. These field and temperature effects can also be seen in R_{max}, the maximum reflectivity of the Bragg peak, as shown in Fig. 1. Since $n_{\mathrm{LCeff}} > n_s$ the LC-silica index contrast increases monotonically with n_{LCeff}. Hence the field-induced reduction in n_{LCeff} is accompanied by a decrease of R_{max}, plotted in Fig. 1C.

The response of λ_B, n_{LCeff}, and R_{max} for *parallel* alignment at $T = 45$ °C is shown in Fig. 2. The open circles are for increasing E and are maintained if the increase of E is stopped and held constant. However, the electro-optic response of the opal/LC composite is highly hysteretic, as is also indicated in Fig. 2. The inset shows the dynamic R_{max} response of a 9 μm thick opal/LC cell to the indicated, (dotted line) transient ac field. R_{max} decreases with increasing E maintaining its change once E is held constant,

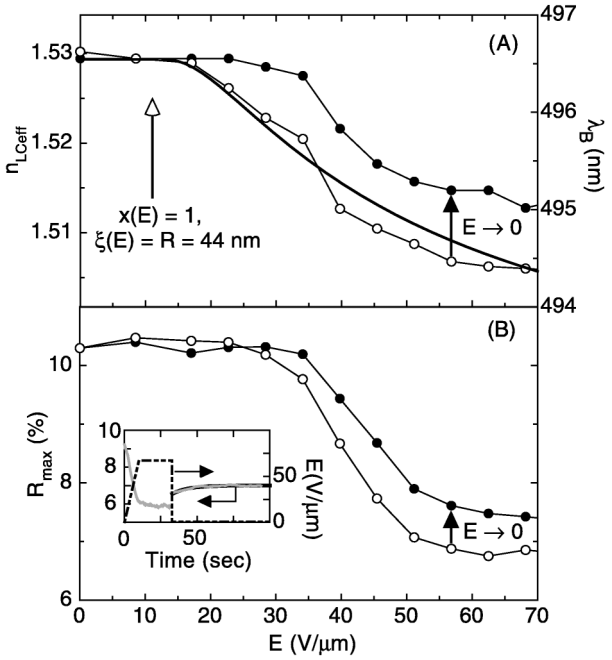

FIG. 2. Field dependence and hysteresis of (A) n_{LCeff} and λ_B and (B) R_{max} for *parallel* alignment. Increasing E reduces n_{LCeff} (open circles), which reduction is only partially reversible (solid circles). The black line is the model calculation of reorientation within a sphere, for a sphere radius $R = 44$ nm. The field response threshold occurs when the penetration length $\xi(E)$ becomes comparable to R. Inset: The typical hysteretic dynamic response (gray line) has fast (<100 msec) and slower relaxation components when the field is removed. The black line is the fit with relaxation time ~11 sec.

but only partially recovers its initial value when $E \rightarrow 0$. The gray curve shows the remnant values of $R_{\max}$ once $E \rightarrow 0$, indicating a significant hysteresis, which is very long-lived in the nematic. The dynamics of the $E \rightarrow 0$ response has a fast component shorter than the 100 msec time response of the spectrometer and a slower component, lasting several tens of seconds. The starting values are recovered only upon heating into the isotropic phase and cooling back into the nematic.

In order to model the effects of LC surface alignment we must extend the theoretical analysis of opal/LC photonic materials [9] to include nonuniform LC orientational ordering. LC order is governed by the bulk elastic energy $U_b(\mathbf{n}) = 1/2K_{ijkl}\nabla_i n_j \nabla_k n_l$, representing the cost of spatial variation of $\mathbf{n}(\mathbf{r})$ (splay, twist, and bend with elastic constants K_S, K_T, and K_B) [19] and the surface energy $U_s(\mathbf{n}) = 1/2\gamma|\mathbf{n} \cdot \mathbf{s}|^2$, where $\gamma > (<) 0$ for the *parallel* (*normal*) case, and $|\gamma|$ characterizes the surface interaction strength. For typical amorphous silica or surfactant surfaces [20], the surface extrapolation length, $\Lambda = K/\gamma > 500$ Å [19], can be small compared to the void size, i.e., the surfaces can be strong enough to establish the surface-preferred pattern of $\mathbf{n}(\mathbf{r})$ in the voids. In this limit confinement in the void space imposes dense topological disorder on $\mathbf{n}(\mathbf{r})$, as illustrated in Fig. 3 for the cases where $\mathbf{n}(\mathbf{r})$ is either *parallel* (A) or *normal* (B) to the sphere surfaces.

In this drawing each sphere is represented by the inscribed cubooctahedron having as its vertices the contact points of the sphere with its nearest neighbors. The LC orientation on the sphere surfaces is conveniently visualized by projecting $\mathbf{n}(\mathbf{r})$ (red) onto the surface polygons (blue squares and blue triangles) of the cubooctahedra. The voids in an fcc close packing are of only two types, made by either four spheres, comprising 28% of the void volume, or six spheres, comprising 72% of the void volume. Once the spheres are represented by cubooctahedra, these voids are represented, respectively, by octahedra and by cubooctahedra, the face of which is either a portion of sphere (blue) or a passage to neighboring voids (yellow), as shown in Fig. 3.

For *parallel* alignment we assume that $\mathbf{n}(\mathbf{r})$ is parallel to but otherwise free to reorient on the silica surface. In this case $\mathbf{n}(\mathbf{r})$ on the spheres is controlled by the contact regions, $U_b(\mathbf{n})$ being minimized when the deformation near each contact point is bent and $\mathbf{n}(\mathbf{r})$ is tangent to circles centered on the contact points, as shown in Fig. 3A. For $\mathbf{n}(\mathbf{r})$ *normal* to the sphere surface (red dots in Fig. 3B) the orientation on the solid surface is unique, imposing a $-\pi$ disclination line to pass from void to void through every yellow triangle. These lines pass through the yellow triangular faces, from one face to another in the octahedra, or to hyperbolic point defects in each cubooctahedron center, as shown in Fig. 3B.

A model for understanding the response of such $\mathbf{n}(\mathbf{r})$ structures to the applied field can be based on the assumption that the LC is to be confined to a volume with a fixed boundary condition on its "surface," S. A field will orient the portion of any such volume $\Omega_{s>\xi(E)}$ which is a distance $s > \xi(E)$ from S, where $\xi(E) = \sqrt{K/\Delta\varepsilon E_{\mathrm{LC}}^2} = 0.33V/E_{\mathrm{LC}}$ is the electric field penetration length [8,19], using $K = 12$ pN as the mean nematic elastic constant for

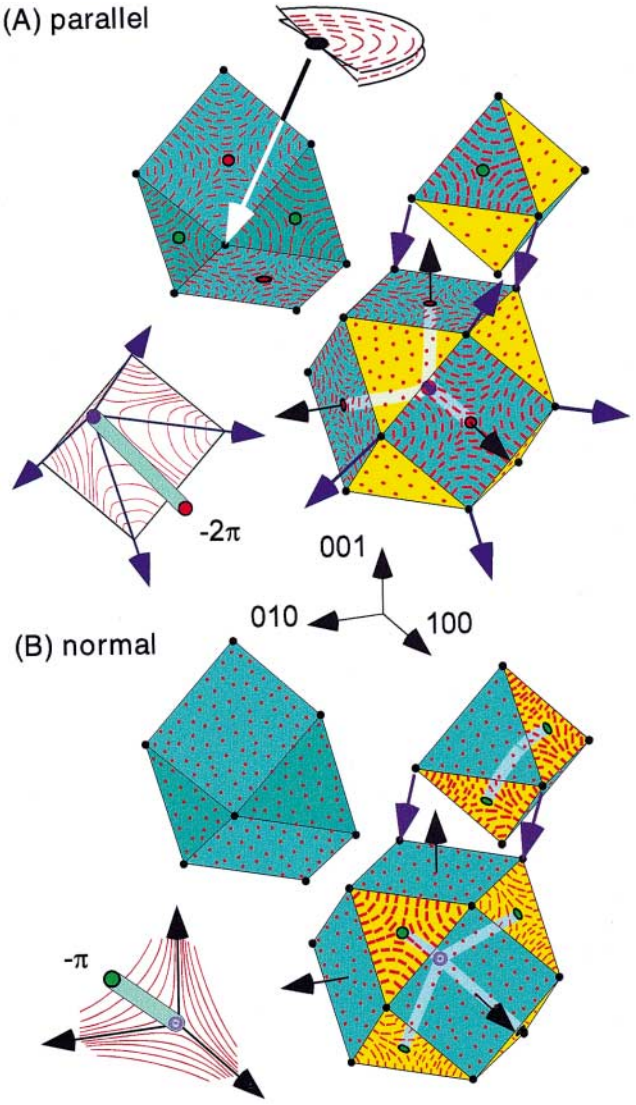

FIG. 3 (color). Nematic LC structure in the periodic contiguous void space of a fcc packing of spheres in contact in the limit of strong LC anchoring. The sphere surfaces (blue) are represented as their inscribed cubooctahedra having the contact points with neighboring spheres as vertices. In this case the fcc voids bounded by four spheres and six spheres are represented, respectively, as octahedra and as cubooctahedra, and fit together as indicated. The void surfaces then consist of elements of sphere surfaces (blue polygons) and passages to neighboring voids (yellow polygons) and have the indicated director distributions $\mathbf{n}(\mathbf{r})$ on them in the parallel (A) and normal (B) cases. The disclination line density and the maximum dimensions of the field responsive regions (bounded by the sphere surfaces and disclination lines) are about the same in the parallel and normal cases, indicating that they should have comparable field response when the LC anchoring is strong.

PCH5 [16], and E_{LC} is the electric field in the LC. Since the mean dielectric constant of the LC, ($\langle\varepsilon_{\mathrm{LC}}\rangle \approx 9$) [16], is considerably greater than that of the silica ($\langle\varepsilon_{\mathrm{SiO_2}}\rangle \approx 3$), E_{LC} is reduced relative to the applied field E approximately as $E_{\mathrm{LC}} \approx 3E/(\langle\varepsilon_{\mathrm{LC}}/\varepsilon_{\mathrm{SiO_2}}\rangle + 2) \approx 0.6E$. The resulting volume averaged n_{LCeff} is given by $\langle n_{\mathrm{LCeff}}(E)^2\rangle = (n_o^2\Omega_{s>\xi(E)} + n_{\mathrm{ave}}^2\Omega_{s<\xi(E)})/(\Omega_{s>\xi(E)} + \Omega_{s<\xi(E)})$. The simplest approach to calculate $\langle n_{\mathrm{LCeff}}(E)\rangle$ is to employ a spherical volume for which $\langle n_{\mathrm{LCeff}}(E)^2\rangle = n_o^2[1 - x(E)]^3 + n_{\mathrm{ave}}^2\{1 - [1 - x(E)]^3\}$, with $x(E) \equiv \xi(E)/R = 0.55V/ER$, where R is the volume radius. The fit of such an equation to the parallel data is shown in Fig. 2, yielding a high-field $n_{\mathrm{LCeff}}(E) = 1.486$, which is close to n_o, and a threshold field $E_{\mathrm{th}} = 12.6\ \mathrm{V}/\mu\mathrm{m}$ determined by $x(E_{\mathrm{th}}) = 1$, for an effective radius $R_{\mathrm{parallel}} = 44$ nm. Note that $n_{\mathrm{LCeff}}(E)$ begins to drop from n_{ave} at E_{th} given by $E_{\mathrm{th}} = 0.55V/R$, as indicated. A similar fit to the normal data, which exhibits no field response for $E < 80\ \mathrm{V}/\mu\mathrm{m}$, yields $R_{\mathrm{normal}} < 7$ nm.

In the structures of Fig. 3, the surface S includes the topological defects, which fix $\mathbf{n}(\mathbf{r})$ along their core lines. If we assume that the defects are tethered, then the spherical volumes for calculating $\langle n_{\mathrm{LCeff}}(E)\rangle$ should then fit into the regions bounded by both sphere surfaces and the defect lines, i.e., be tangent to the relevant spheres and lines. In the *parallel* case, the relevant radii are for eight spheres in the cubooctrahedral void centered on [111] lines passing through the void center for which $R = 0.122D = 25$ nm. For E along a [111] direction, $\mathbf{n}(\mathbf{r})$ in two of these spheres is already mostly parallel to E and therefore not switchable. In the other six, which occupy 25% of the total LC volume, $\mathbf{n}(\mathbf{r})$ is oriented at $\sim 70°$ with respect to E and should respond continuously above a threshold of $E_{\mathrm{th}} = 0.55V/R = 22\ \mathrm{V}/\mu\mathrm{m}$. In the *normal* case, the largest spheres, of which there are 12, will be centered on [110] lines that pass through the void center and have a radius $R = 0.115D = 24$ nm. Six of these spheres are bisected by planes on which the director is normal to E and thus will have a higher-E Frederiks-like threshold behavior. In the other six spheres, occupying 20% of the LC volume, $\mathbf{n}(\mathbf{r})$ is oriented at $\sim 35°$ with respect to E and should respond continuously above a threshold of $E_{\mathrm{th}} = 0.55V/R = 23\ \mathrm{V}/\mu\mathrm{m}$. In both the *parallel* and *normal* cases reorientation of $\mathbf{n}(\mathbf{r})$ in other parts of the LC would have a smaller effective radius and thus require higher fields. For both cases the disclinations limit spherical volumes in the octahedral voids to radii $R \lesssim 0.07D = 14$ nm.

The defect structures combined with this estimate indicate that with $\Lambda \ll R$ the *parallel* and *normal* cases have similar structural flexibility and thus should have similar responses to the applied field and serve to illustrate why the *normal* case response is weak, with only 20% of the LC commencing to reorient at $24\ \mathrm{V}/\mu\mathrm{m}$. The observed *parallel* response is thus evidence that for the *parallel* case Λ is significantly larger than for the *normal* case, enabling $\mathbf{n}(\mathbf{r})$ to rotate away from the sphere surface and the nematic elasticity to partially expel the topological disorder, which is maintained by the surface interactions. The effective field threshold radius $R_{\mathrm{parallel}} = 44$ nm for the parallel case is comparable to $R_{\mathrm{cuboct}} = 0.212D = 43.8$ nm, the radius of the largest sphere fitting inside the cubooctahedral voids, indicating that the field can squeeze the remnant topological disorder from these voids. Since the large voids comprise 72% of the total LC volume, this picture is consistent with the leveling of $n_{\mathrm{ave}} - n_{\mathrm{LCeff}}$ vs E at $n_{\mathrm{ave}} - n_{\mathrm{LCeff}} \sim 0.6(n_{\mathrm{ave}} - n_o)$, where $n_{\mathrm{ave}} - n_o$ is the maximum possible change. Such a process should have significant hysteresis, as is observed, and would be highly irregular, with remnant topological structure governed by weak variations in surface interaction or crystal structure. In this case the dynamics and response to field of $\mathbf{n}(\mathbf{r})$ will resemble that of a nematic confined by quenched random disorder [21].

This work was supported by NASA Grants No. NAG 3-2457 and No. NAG 8-1665 and NSF MRSEC Grant No. DMR 98-09555.

*Present address: Department of Electrical Engineering, Soongsil University, Seoul, 156-743, Korea.

[1] E. Yablonovitch, Phys. Rev. Lett. **58**, 2059 (1987); S. John, *ibid.* **58**, 2486 (1987).
[2] *Photonic Band Gap Materials,* edited by C. M. Soukoulis (Kluwer, Dordrecht, 1996).
[3] Special issue on *Photonic Crystals and Photonic Microstructures* [IEE Proc. Optoelectron. **145** (1998)].
[4] A. A. Zakhidov *et al.,* Science **282**, 897 (1998).
[5] N. A. Clark *et al.,* Nature (London) **281**, 57 (1979).
[6] I. I. Tarhan and G. H. Watson, Phys. Rev. Lett. **76**, 315 (1996).
[7] L. K. Cotter and N. A. Clark, J. Chem. Phys. **86**, 6616 (1987).
[8] *Liquid Crystals: Applications and Uses,* edited by B. Bahadur (World Scientific, Singapore, 1990).
[9] K. Busch and S. John, Phys. Rev. Lett. **83**, 967 (1999).
[10] S. W. Leanord *et al.,* Phys. Rev. B **61**, R2389 (2000).
[11] K. Yoshino *et al.,* Appl. Phys. Lett. **75**, 932 (1999).
[12] K. Yoshino *et al.,* Mol. Cryst. Liq. Cryst. A **329**, 1045 (1999).
[13] P. Mach *et al.,* Bull. Am. Phys. Soc. **45**, 767 (2000).
[14] Nissan Chemical Ind., Ltd. MP-2040.
[15] J. Bibbette, J. Colloid Interface Sci. **147**, 474 (1991).
[16] U. Finkenzeller *et al.,* Liq. Cryst. **5**, 313 (1989).
[17] A. A. Sonin, *The Surface Physics of Liquid Crystals* (Gordon and Breach, Philadelphia, 1995).
[18] D. J. W. Aastuen *et al.,* Phys. Rev. Lett. **57**, 1733 (1986).
[19] P. G. deGennes and J. Prost, *The Physics of Liquid Crystals* (Clarendon Press, Oxford, 1993).
[20] L. M. Blinov *et al.,* Liq. Cryst. **5**, 645 (1989).
[21] T. Bellini and N. A. Clark, in *Liquid Crystals in Complex Geometries,* edited by G. P. Crawford and S. Zumer (Taylor & Francis, London, 1996).